Role of Molecular Interactions in Supramolecular Polypeptide–Polyphenol Networks for Engineering Functional Materials

Yiyuan Han,[†] René P. M. Lafleur,[†] Jiajing Zhou,[†,‡] Wanjun Xu,[†] Zhixing Lin,[†] Joseph J. Richardson,[†,§] and Frank Caruso*[,†]

[†]Department of Chemical Engineering, The University of Melbourne, Parkville, Victoria 3010, Australia
[‡]Department of NanoEngineering, University of California San Diego 9500 Gilman Dr., La Jolla, CA 92093, USA
[§]Department of Materials Engineering, School of Engineering, University of Tokyo, Tokyo 113−8656, Japan
*Corresponding author. E-mail: fcaruso@unimelb.edu.au

ABSTRACT: Supramolecular assembly affords the development of a wide range of polypeptide-based biomaterials for drug delivery and nanomedicine. However, there remains a need to develop a platform for the rapid synthesis and study of diverse polypeptide-based materials without the need for employing complex chemistries. Herein, we develop a versatile strategy for creating polypeptide-based materials using polyphenols that display multiple synergistic cross-linking interactions with different polypeptide side groups. We evaluated the diverse interactions operating within these polypeptide–polyphenol networks via binding affinity, thermodynamics, and molecular docking studies and found that positively charged polypeptides (K_a of ~2×10^4 M^{-1}) and polyproline (K_a of ~2×10^6 M^{-1}) exhibited stronger interactions with polyphenols than other amino acids (K_a of ~2×10^3 M^{-1}). Free-standing particles (capsules) were obtained from different homopolypeptides using a template-mediated strategy. The properties of the capsules varied with the homopolypeptide used: e.g., positively charged polypeptides produced thicker shell walls (120 nm) with reduced permeability and involved multiple interactions (i.e., electrostatic and hydrogen), whereas uncharged polypeptides generated thinner (10 nm) and more permeable shell walls due to the dominant hydrophobic interactions. Polyarginine imparted cell penetration and endosomal escape properties to the polyarginine–tannic acid capsules, enabling enhanced delivery of the drug doxorubicin (2.5 times higher intracellular fluorescence after 24 h) and a corresponding higher cell death in vitro when compared with polyproline–tannic acid capsules. The ability to readily complex polyphenols with different types of polypeptides suggests that a wide range of functional materials can be generated for various applications.

INTRODUCTION

Advances in synthetic chemistry have enabled the synthesis of diverse biopolymers that can bridge the gap between materials science and biology via regulating biointerfaces.[1] This progress has led to the rapid development of nanomaterials for various biomedical applications including disease diagnosis, drug/gene delivery, and tissue engineering.[2–6] Synthetic polypeptides (PPeps) and poly(amino acids), which are composed of amino acids, have emerged as a platform for engineering nanomaterials owing to their facile synthesis, tunable composition, and well-defined sequence and corresponding physicochemical properties.[7] Moreover, PPeps mimic endogenous macromolecules and thereby exhibit excellent biocompatibility and biodegradability as well as tunable biofunctionality.[8–10] For instance, polyarginine (PArg) is commonly used as a cell-penetrating peptide for intracellular delivery[11,12] and elastin-like PPep-based hydrogels are often used to mimic the extracellular matrix in synthetic biomaterials.[13] In this context, PPep-based materials are generally constructed using different covalent-linking molecules to bridge the PPeps, thereby producing robust functional assemblies.[2,14] However, such strategies require complex synthetic steps and toxic cross-linking agents, and yield irreversible bonds, which collectively limit the broad use of PPeps as a platform for engineering biomedical materials and advanced therapeutics.

Supramolecular interactions have evolved into a toolbox for designing molecular recognition motifs and for driving self-assembly among discrete building blocks.[15–17] The rational design of PPep-based materials that can incorporate other functional molecules through noncovalent interactions allows for the generation of complex assemblies with synergistic and emergent physicochemical properties, thereby expanding the versatility of such systems.[18–21] For example, noncovalent dynamic supramolecular complexes formed between PPeps and complementary molecules, such as polymers (e.g., polyethylenimine), chemotherapeutic drugs, and biomacromolecules (e.g., nucleotides), have recently been explored as carrier systems for the delivery of a wide range of functional cargos.[22–25] Naturally occurring polyphenols show potential as supramolecular building blocks for engineering biomaterials in diverse fields,[26–28] and it has been shown that polyphenols can simultaneously exhibit a variety of supramolecular interactions with biomacromolecules, in particular proteins, without disrupting their functions.[29,30] The essential interactions governing supramolecular assembly between polyphenols and proteins are, however, still elusive. We therefore envision that a systematic investigation into how homopolypeptides and polyphenols interact not only will unravel the reciprocal interactions between proteins/PPeps and polyphenols but also can help elucidate principles for the rational design of PPep-based materials with desired properties for wider applications.

In the present study, we report a general approach to design supramolecular PPep–polyphenol networks (PPNs) and demonstrate the rational design of PPN materials with customized properties and functions for bioapplications. Both charged and uncharged homopolypeptides (i.e., polylysine (PLys), PArg, polyhistidine (PHis), polyglutamic acid (PGlu), polythreonine (PThr), polyproline (PPro), and polyalanine (PAla)) were selected for studying the intermolecular interactions of PPeps with polyphenols such as tannic acid (TA) (Figure 1a). Specifically, the molecular binding kinetics and thermodynamic parameters between PPeps and polyphenols were measured experimentally, with the results corresponding well with the molecular docking simulations. The complexation between the PPeps and polyphenols was rationalized based on the various interactions between polyphenols and the side chains of the different PPeps. These insights further allowed us to synthesize hollow PPN capsules using sacrificial templates, demonstrating the possibility to create free-standing PPN materials with well-defined nanostructures and structural complexity (Figure 1b). The different types of PPeps employed endowed the resulting PPN capsules with different physicochemical properties, thus affording control over surface charge, microstructure, film thickness, and stimuli-responsive behavior. For example, the PArg–TA PPN capsules showed a higher cellular association than the other PPNs and underwent endosomal escape due to their pH-responsive charge reversal property. In addition, the PPep–TA capsules could serve as intracellular drug delivery platforms owing to the universal adherence of TA to other molecules that allowed for the controlled loading and release of therapeutic cargo (e.g., doxorubicin).

RESULTS AND DISCUSSION

To investigate the intermolecular interactions between PPeps and polyphenols, seven homopolypeptides with different side chains (i.e., PLys, PArg, PHis, PGlu, PThr, PPro, and PAla) were chosen as model PPeps (Table S1), while TA was selected as the model polyphenol. First, quartz crystal microbalance (QCM) gravimetry was used to detect and monitor the molecular binding kinetics in real-time by measuring changes in the frequency of a quartz crystal resonator.[31] Specifically, a layer of TA was deposited on the gold-coated QCM crystals and subsequently the binding of the seven PPeps was monitored at pH values of 4.0 and 7.4. For the charged PPeps, distinct frequency changes were observed after the addition of PLys or PArg at both pH values, whereas no distinct changes were observed after the addition of PGlu at either pH values and the addition of PHis resulted in strong interactions at pH 4.0 only (Figure 1c,d). The PPep-to-TA mass ratios were then calculated and plotted (Figure 1e), with the results indicating that the PPeps with charged side chains exhibited pH-responsive binding with TA. Specifically, PPeps with positively charged side chains showed increased binding to TA at neutral pH (7.4) than at acidic pH (4.0). This is likely caused by the deprotonation of TA at neutral pH. In contrast, the negatively charged PGlu showed slightly increased binding at the lower pH, likely because the protonation of PGlu below pH 4.0 reduced the electrostatic repulsion with TA, and thereby allowed for hydrogen bonds to form. PHis was soluble at pH 4.0 only and showed high affinity for TA at that pH. PPeps that contain uncharged and hydrophobic side chains, namely PThr, PPro, and PAla, were also investigated. Among these three PPeps, PPro showed the strongest binding to TA, which is likely caused by strong aromatic–proline interactions (Figure 1f),[32] whereas PAla showed the weakest binding to TA (Figure 1g). Negligible differences were observed when comparing the binding behavior of each peptide at pH values 4.0 and 7.4 (Figure 1h), suggesting that hydrogen bonding was minimal between TA and the uncharged PPeps.

Isothermal titration calorimetry (ITC) was used to determine the thermodynamics of the interactions between PPeps and TA. For these measurements, TA solutions loaded in the injection syringe were titrated into different PPep solutions in sample cells. The heat change was monitored and then plotted as a function of the molar ratio of the PPeps and TA (Figure 1i,j and Figure S1) and all fitted thermodynamic parameters (i.e., association constant (K_a), binding constant (K_d), enthalpy change (ΔH), entropy change (ΔS), Gibbs free energy change (ΔG), and $T\Delta S$, where T is the temperature) are provided in Table S2. Binding between positively charged PArg and TA was predominantly enthalpy driven with a high ΔH of -76.40 ± 4.12 kcal mol^{-1} and an unfavorable entropic contribution ($-T\Delta S = 70.63$ kcal mol^{-1}), implying that an equilibrium between enthalpic and entropic contributions prevailed. In contrast, the binding between PPro and TA showed an unfavorable enthalpy ($\Delta H = 4.25$ kcal mol^{-1}) and a favorable entropy ($-T\Delta S = -12.69$ kcal mol^{-1}), which was consistent with a hydrophobic association process.[34] Importantly, all examined PPeps that complexed with TA showed a negative ΔG (Figure 1k), indicating that association is spontaneous. Specifically, the thermodynamic parameters reveal that PArg, PHis, and PPro, complex with TA with a relatively higher K_a of 1.95×10^4, 2.39×10^4, and 1.56×10^6 M^{-1}, respectively, whereas PGlu, PAla, and PThr complex with a relatively lower K_a of 5.11×10^3, 3.53×10^3, and 1.12×10^3 M^{-1}, respectively (Table S2). These K_a values represent moderate affinities (10^3–10^8 M^{-1}) and are ideal for self-assembly, confirming the potential for developing self-assembled materials from PPeps and TA.[35]

To understand the interaction sites between PPeps and polyphenols, mixtures of PPeps and polyphenols were analyzed using ^{1}H-NMR spectroscopy. Epigallocatechin gallate (EGCG) was substituted for TA in this analysis, as EGCG is a simpler molecule with comparable phenolic moieties, whereas TA is composed of a mixture of molecules that makes careful analysis difficult (Figure S2). As observed from Figure S3, the interaction of PArg with EGCG resulted in different chemical shifts of the H atoms closest to the guanidine group on the arginine side chain, suggesting that PArg interacts with polyphenols via the guanidino group on the side chains. Interestingly, the ^{1}H-NMR spectra of mixtures of PPro and EGCG at different molar ratios consistently featured peaks of at least one of the molecules (Figure S4), likely because an excess of either

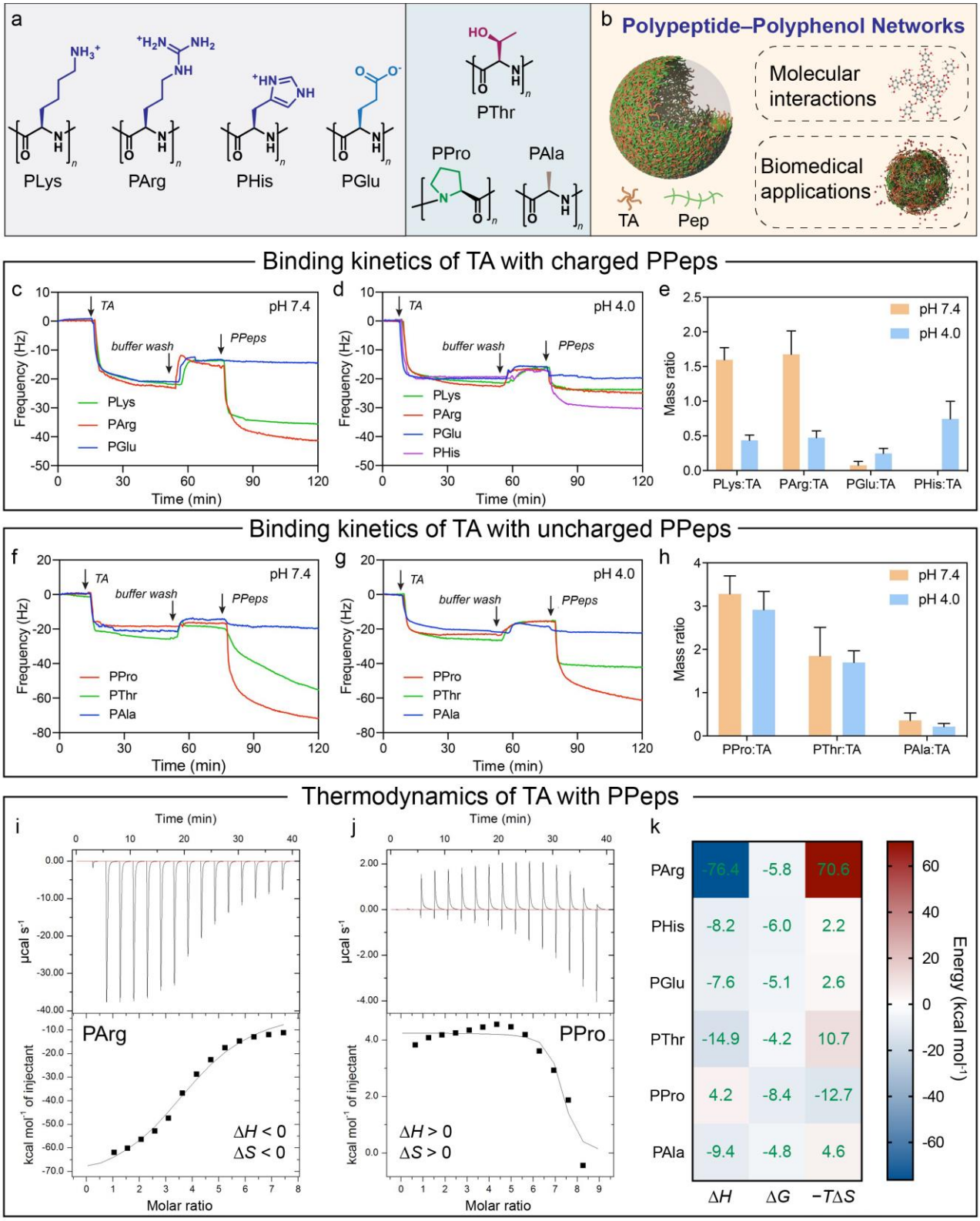

Figure 1. (a) Chemical structures of the seven PPeps investigated in this study. (b) Illustration of PPep–polyphenol networks (PPNs) for biomedical applications; the PPNs are formed by interactions between TA and PPep. (c–e) Binding kinetics of TA with charged PPeps at pH 7.4 (c) and pH 4.0 (d), as monitored by QCM, and the corresponding binding mass ratios, as calculated using Sauerbrey equation[33] (e). PHis does not dissolve in pH 7.4 buffer; therefore data could only be obtained at pH 4.0. (f–h) Binding kinetics of TA with uncharged PPeps at pH 7.4 (f) and pH 4.0 (g), as monitored by QCM, and the corresponding binding mass ratios (h). (i,j) Thermodynamic ITC curves obtained by titration of PArg (i) or PPro (j) in TA at 25 °C. The top panels represent the raw data and the bottom panels display the fitted curves of changes in the molar heat as a function of PPep-to-TA molar ratio. (k) Summary of thermodynamic parameters (ΔH, ΔG, $-T\Delta S$) determined from ITC analysis.

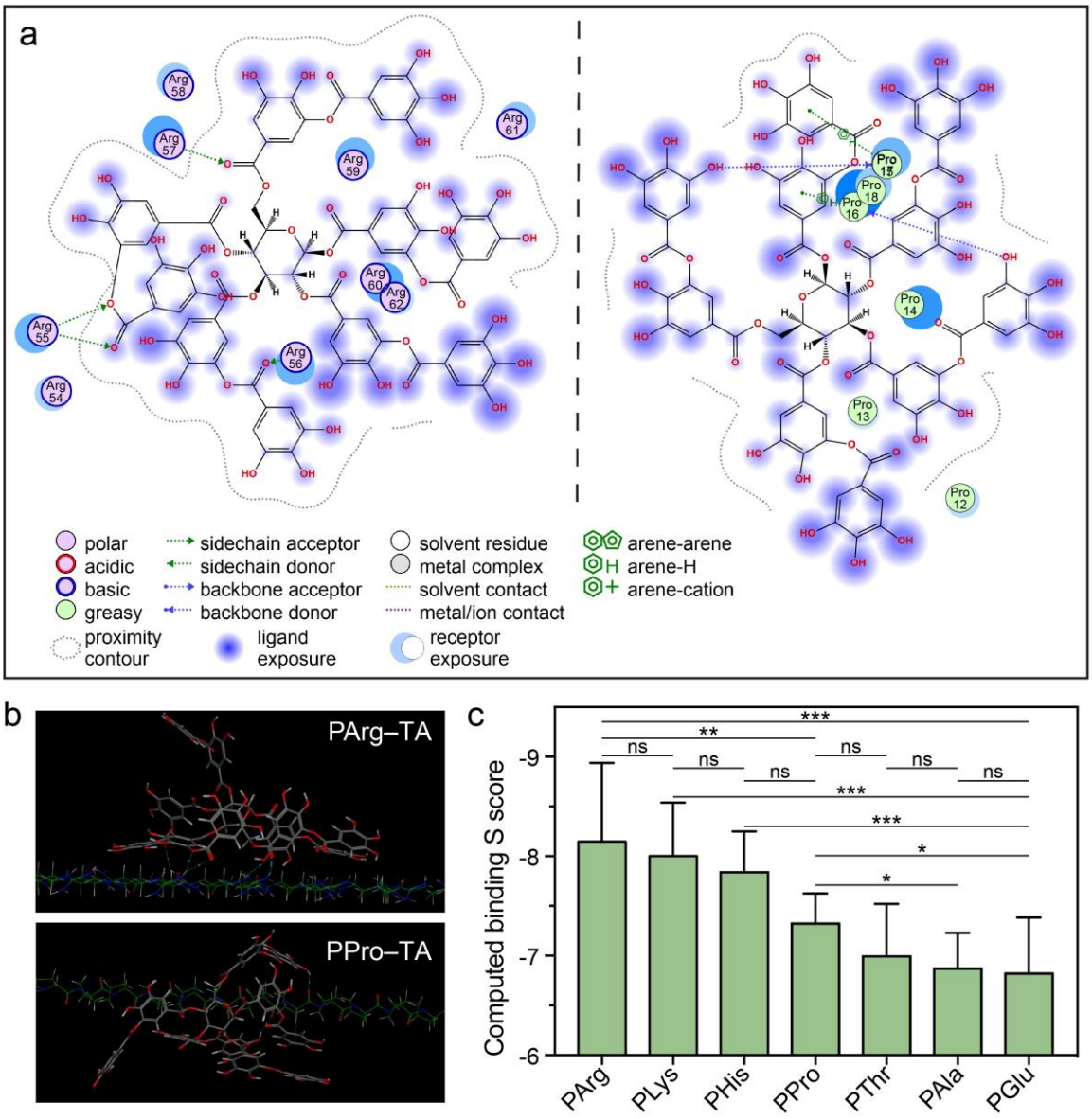

Figure 2. (a) 2D Ligand interaction diagrams for docking TA to the binding site of PArg or PPro using MOE software. (b) Side-view of 3D molecular interactions between PArg or PPro with TA visualized by MOE software. (c) Computed binding S scores for the interactions between different PPeps and TA evaluated by MOE software. Data represent the mean ± standard deviation of three configurations. Statistical significance was determined by an unpaired *t*-test and is reported as ***$p < 0.001$, **$p < 0.01$, *$p < 0.05$, ns $p > 0.05$.

molecule can mask the other. These findings indicate that the interactions between PArg or PPro and EGCG are sufficiently robust for assembly.

To further study the interactions between the PPeps and TA, we performed molecular docking simulations using Molecular Operating Environment (MOE) software.[36] The two dimensional (2D) ligand interaction diagrams of two representative PPeps (i.e., PArg and PPro) with TA demonstrated that PArg prefers to interact with the ester and carbonyl groups of TA, whereas PPro interacts with both the hydroxyl groups and aromatic rings of TA (Figure 2a). The three-dimensional (3D) molecular interaction graphics showed that the interactions between PArg and TA occur between the side chains of PArg and the periphery of TA. In contrast, PPro is surrounded by TA molecules in a different manner (Figure 2b). The 2D ligand interaction diagrams of the remaining PPeps with TA are shown in Figure S5. To obtain a clear understanding of this information, all-atom MOE docking was performed on TA for each PPep and the binding S scores were computed based on binding affinities with all possible binding geometries. PPeps with lower S scores tend to establish a stronger interaction with TA.[37] Among all examined PPeps, the positively charged PPeps (i.e., PArg, PLys, and PHis) showed the lowest S scores (−8.15, −8.00, and −7.84, respectively), and among all the uncharged PPeps, PPro showed the lowest S score (−7.32) (Figure 2c), which agrees with the experimental analytical results. We note that there are no significant differences between the S scores of most PPeps from the same class (charged or uncharged) as their binding strengths are approximated. However, the observed trend in the S scores of the examined PPeps is consistent with the experimental observations on PPNs. Collectively, these findings demonstrate how different types of interactions between PPeps and polyphenols at the molecular level can contribute to complexation.

We assessed the suitability of PPeps and polyphenols to assemble into free-standing PPN films (capsules) using a sacrificial template (Figure 3a), which would enable the encapsulation of functional molecules relevant for drug delivery.[38,39] TA and PPeps were added to a suspension containing $CaCO_3$ particles of 3 μm in diameter. Following incubation for 4 h, the $CaCO_3$ templates were removed using ethylenediaminetetraacetic acid.[29] The PPeps that showed strong binding to TA resulted in the formation of hollow capsules, namely the PPeps with positively charged side chains PLys, PArg, and PHis, and the PPeps with uncharged side chains PPro and PThr. Monodisperse PPep–TA capsules were observed using differential interference contrast (DIC) microscopy, and fluorescent capsules were assembled using fluorescein isothiocyanate (FITC)-labeled PPeps and visualized by confocal laser scanning microscopy (CLSM) (Figure 3b). The UV–vis spectra of the PArg–TA and PPro–TA capsules were different from the UV–vis spectra of the respective free PPeps and TA components (Figure S6). The Fourier transform infrared (FTIR) spectrum of the PPro–TA capsules demonstrated peak overlaps with the spectra of free TA and PPro (Figure S7). Both the UV–vis and FTIR results confirm the presence of both compounds in the PPep–TA capsules. The ζ-potential results showed that the surface charge of all the formed capsules varied depending on the PPep type (Figure 3c). Specifically, the capsules formed from positively charged PPeps (i.e., PLys, PArg, PHis) demonstrated pH-responsive charge reversal behavior that could potentially allow them to act as stimuli-responsive drug delivery carriers.

Two representative PPeps, PArg and PPro, were chosen to characterize the structure and properties of the formed PPN capsules in detail. Although prepared in the same way, microscopy analysis showed that the PPro–TA and PArg–TA capsules had a different structure and thickness. The wall thickness of the PPro–TA capsules was ~10 nm (Figure 4a–c), whereas a single wall of the PArg–TA capsules was ~120 nm thick (Figure 4d–f). Scanning electron microscopy (SEM) and atomic force microscopy (AFM) performed on air-dried capsules revealed that the PPro–TA capsules exhibited surface features with folds and creases typical to collapsed thin film capsules.[40,41] In contrast, air-dried PArg–TA capsules showed a toroidal shape with solid and self-sustaining walls. Moreover, the PPro–TA and PArg–TA capsules exhibited different permeability and disassembly kinetics in various media (Figure 4g,h). To investigate the permeability of the capsules, they were loaded with FITC-dextran of different molecular weights (ranging from 20 to 2000 kDa) and visualized in solution using CLSM. The PPro–TA capsules with thinner shells appeared to be more permeable than the PArg–TA capsules with thicker shells. For instance, nearly 100% of the PPro–TA capsules were permeable to 500 kDa FITC-dextran, whereas only around 15% of the PArg–TA capsules were permeable (Figure 4g). Subsequently, the disassembly of fluorescent capsules was monitored after the addition of molecules that are expected to compete with the interactions operating between the PPeps and TA. Urea was used to compete with hydrogen bonding, Tween 20 for hydrophobic interactions, and guanidinium chloride (GdmCl) for electrostatic interactions. The intact fluorescent capsules remaining after incubation were then counted using flow cytometry. The PPro–TA capsules disassembled completely in Tween 20 but largely remained intact in the presence of urea, and only some disassembled in GdmCl, indicating that the dominant interaction is hydrophobic. In contrast, PArg–TA capsules partially disassembled in urea and GdmCl but mostly remained intact in the presence of Tween 20, indicating that hydrogen bonding and electrostatic interactions both contribute to the network stability (Figure 4h). Diverse interactions between different PPeps and polyphenols offer the possibility to fabricate PPep materials with distinctive physicochemical properties, structures, and stimuli-responsive behaviors, and this platform could be extended to smart delivery systems for various biomedical applications.

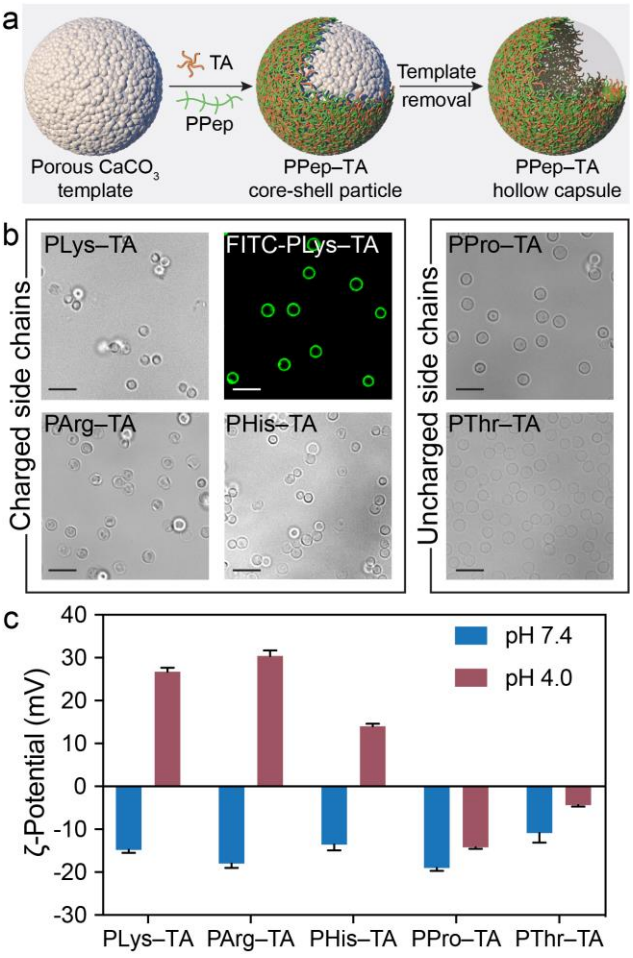

Figure 3. (a) Schematic of the formation of PPep–TA core-shell particle and hollow capsule. (b) DIC microscopy and fluorescence microscopy images of different PPep–TA capsules. Scale bars: 10 μm. (c) ζ-potentials of different PPep–TA capsules measured under different pH conditions. Data are shown as the mean ± standard deviation (n = 3).

The cell association and endosomal escape behaviors of PPNs were examined to explore their potential for biomedical applications. For the studies, green-fluorescent polystyrene (PS) particles of 1 μm in size were coated with PPArg–TA, PPro–TA, or TA, as confirmed by ζ-potential measurements (Figure S8). As observed from Figure 5a,b, both the PArg–TA coatings and PPro–TA coatings facilitated

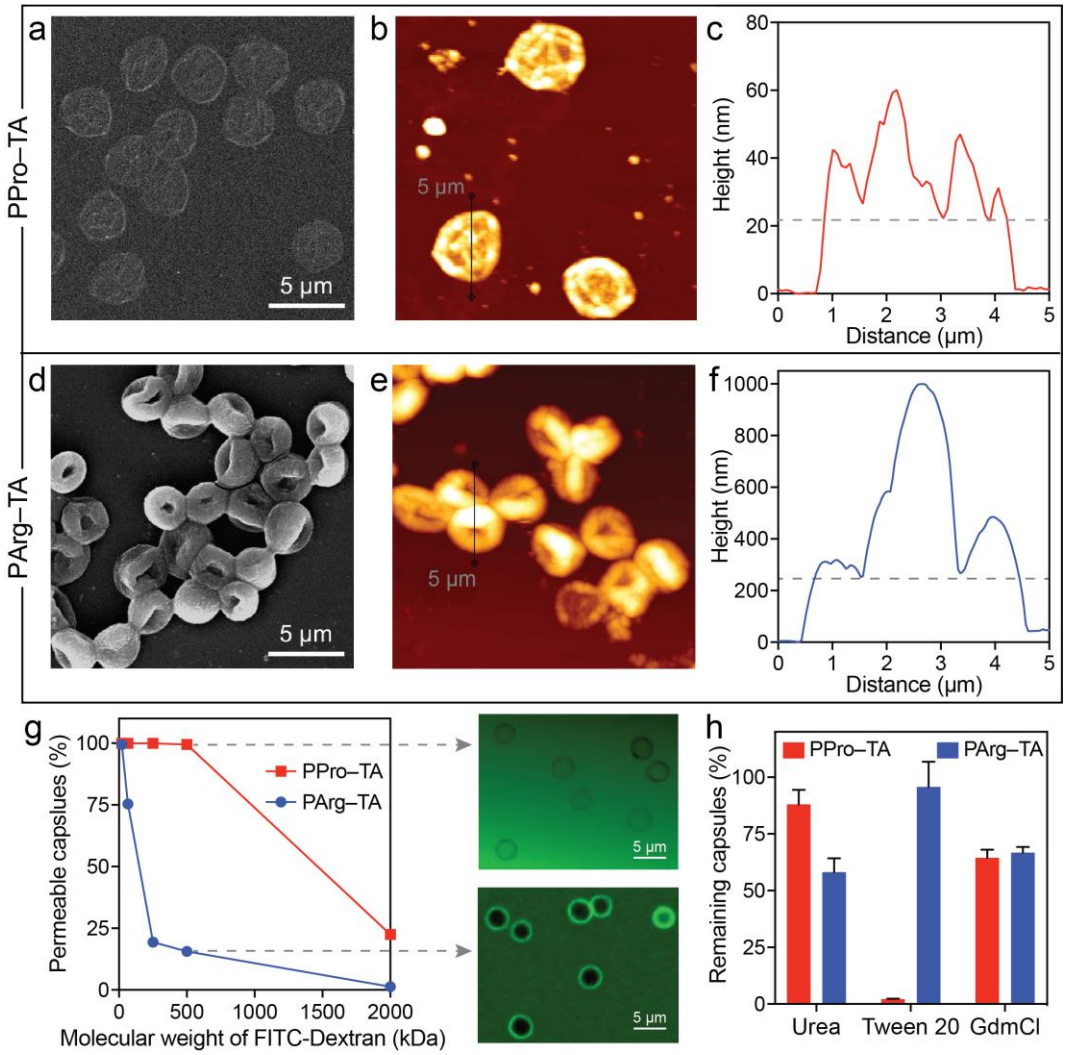

Figure 4. (a,d) SEM images, and (b,e) AFM images and (c,f) corresponding height measurements of the PPro–TA (a–c) and PArg–TA (d–f) capsules. (g) Percentage of PPep–TA capsules permeable to FITC-dextran of different molecular weights and corresponding CLSM images of PPep–TA capsules incubated with 500 kDa FITC-dextran at pH 7.4 for 10 min. The permeability of 100 capsules was measured using CLSM. (h) Interaction-dependent disassembly of PPep–TA capsules in the presence of 100 mM of urea, tween 20, or GdmCl after 24 h, as assessed by flow cytometry. Data are shown as the mean ± standard deviation of three independent experiments.

the cellular association of the particles, which was not the case for the TA control groups. As arginine-rich peptides and proline-rich peptides are cell-penetrating peptides, this finding indicates that the assembled materials can retain the functions of the constituent peptides. Specifically, the PArg–TA particles showed ~70% cell association at a high cell-to-particle ratio (1:100) after incubation for 1 h, whereas the PPro–TA particles showed ~30% cell association under the same conditions. At a lower cell-to-particle ratio of 1:10 and after incubation for 1 h, the PArg–TA particles showed ~20% cell association, whereas the PPro–TA particles showed low association (~4%) similar to the control group (~3%). Additionally, PArg–TA particles demonstrated increased cell association after longer incubation times (2 h), reaching ~80% cell association at a cell-to-particle ratio of 1:100, whereas increases in cell association of other particles were not obvious. These findings demonstrate the stronger cellular association displayed by PArg–TA particles when compared to PPro–TA particles, which is likely due to the high cell-binding and cell-penetrating activity of the positively charged peptides (arginine) in comparison with amphipathic peptides (proline).

The intracellular fate of the particles was subsequently examined by incubating the PPep–TA-coated PS particles with HeLa cells for 4 h. From the CLSM analyses, we found that a portion of the internalized PArg–TA-coated PS particles (green) were not colocalized with acidic compartments such as the endosomes and lysosomes (red) but were found at other locations in the cytosol (Figure 5c and Figure S9). In contrast, the PPro–TA-coated PS particles inside the cells were completely trapped within the endosomes and lysosomes (Figure 5c and Figure S9). The control PS particles that were coated with TA showed a similar endosomal entrapment feature to PPro–TA (Figure S10). These results suggest that PArg–TA coatings can facilitate the escape of particles from endosomes and lysosomes, probably due to the pH-responsive charge reversal behavior of the PArg–TA assemblies (Figure 3c) or the cell-penetrating nature of PArg. The diversity of intracellular distribution of the examined PPep–TA particles suggests that the rational design of hybrid

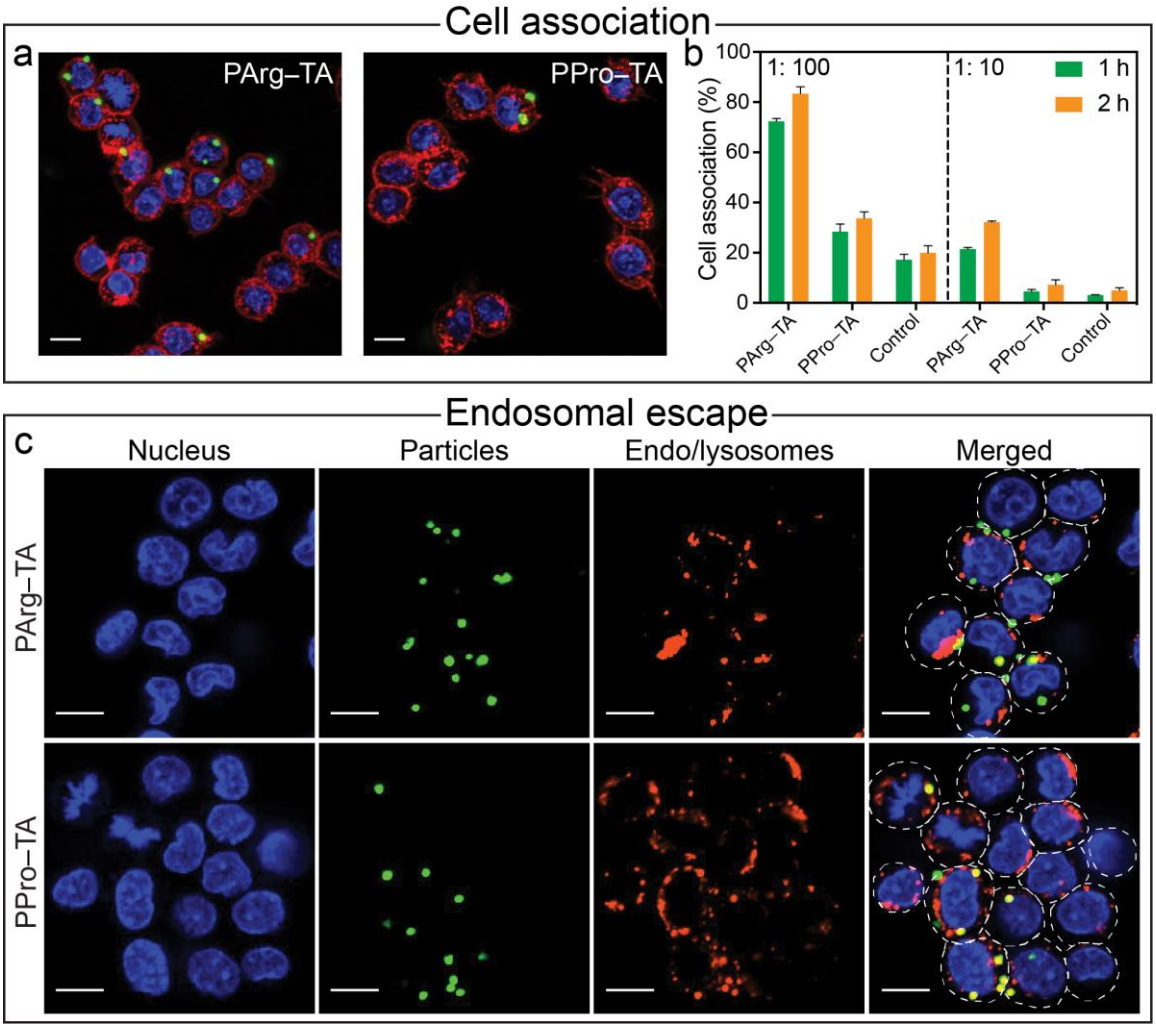

Figure 5. (a) CLSM images of PArg–TA and PPro–TA particles incubated with HeLa cells for 1 h. Scale bars: 10 μm. (b) Percentage of HeLa cells associated with PArg–TA or PPro–TA particles, and TA-coated particles (control) after incubation for 1 or 2 h, as assessed by flow cytometry. The cell-to-particles ratio was 1:100 or 1:10. Data are shown as the mean ± standard deviation of three independent experiments. (c) CLSM imaging of a LysoTracker colocalization assay performed in HeLa cells after incubation for 4 h with PArg–TA or PPro–TA particles. The cell-to-particle ratio was 1:50. Scale bars: 10 μm.

PPep–TA assemblies might lead to tailored intracellular transport, which is important for advanced drug delivery.[42]

To evaluate the potential of PPN capsules for drug delivery applications, anticancer drug doxorubicin (Dox) was preloaded into $CaCO_3$ template particles and Dox-loaded PPN capsules were synthesized (Figure S11). The in vitro drug release in phosphate-buffered saline buffer was first studied. Both the PArg–TA and PPro–TA capsules gradually released Dox over 48 h (Figure S12). Capsules were then prepared using Alexa Fluor (AF) 488-labeled PPeps (PArg and PPro) to visualize the intracellular delivery in detail by CLSM (Figure 6a). PC3 cells incubated with Dox-loaded PPro–TA capsules for 24 h displayed a weak Dox fluorescence (red). In comparison, a strong Dox fluorescence (red) was observed inside the PC3 cells following 24 h incubation with Dox-loaded PArg–TA capsules. The corrected total cell fluorescence (CTCF) intensity was calculated for the cells treated with both capsules. The cells treated with Dox-loaded PPro–TA capsules exhibited a relatively lower intensity (~1.8×10^6), whereas the cells treated with Dox-loaded PArg–TA capsules showed higher intensity (~4.6×10^6), which confirmed their effective internalization and drug release in cancer cells (Figure 6b). Next, we incubated PC3 cells with Dox-loaded capsules and free Dox at different doses for 48 h and investigated cell viability (Figure 6c). Cell viability decreased as the concentration of Dox increased for both capsule and control groups. The results demonstrated that both PArg–TA and PPro–TA capsules induced anticancer activity (~26% and ~36% cell viability at a dose of 1 μg Dox, respectively). The efficiency of PArg–TA was higher than PPro–TA at the same dose of Dox, which is likely due to the successful endosomal escape of PArg–TA. PPep–TA capsules that were not loaded with Dox did not show cell toxicity toward PC3 cells after incubation for 48 h (Figure S13). To improve reproducibility, reporting, and reanalysis, this study conforms to the Minimum Information Reporting in Bio–Nano Experimental Literature (MIRIBEL) standard,[43] and a companion checklist is provided in the Supporting Information.

CONCLUSION

We have comprehensively studied various aspects of PPNs, from fundamentals, including molecular interactions, to the fabrication of functional materials. Investigations into

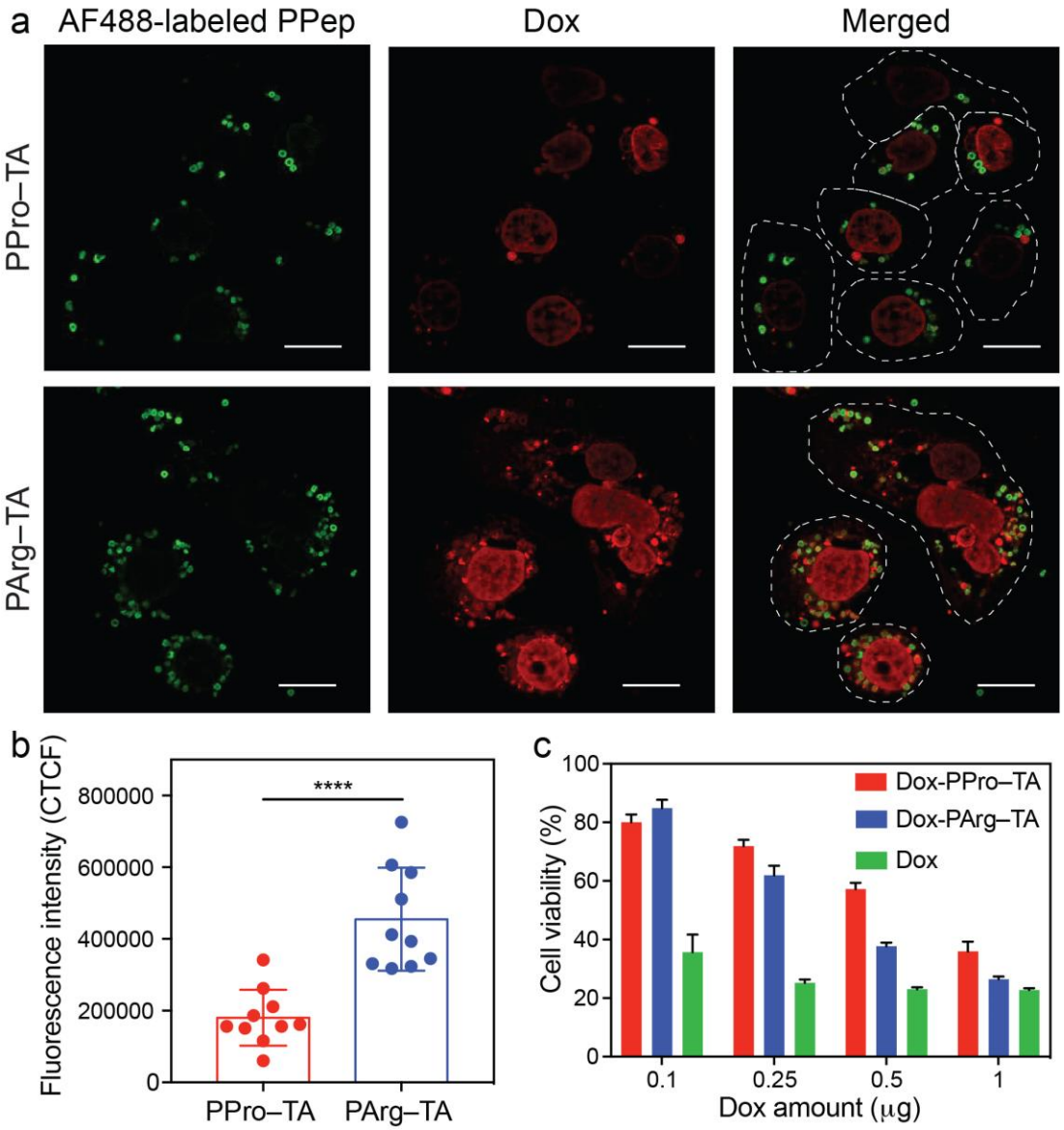

Figure 6. (a) CLSM imaging of Dox-loaded PPep–TA capsules incubated with PC3 cells for 24 h. PPeps are labeled with AF488 dye (green). Scale bars: 20 μm. (b) Quantification of fluorescence intensity in cells incubated with Dox-loaded PPep–TA capsules. CTCF is calculated by subtracting the contribution of the background from the integrated fluorescence density within the regions of interest. Data represent the mean ± standard deviation of 10 measurements. Statistical significance was determined by an unpaired *t*-test and is reported as ****$p < 0.0001$. (c) Viability of PC3 cells incubated with Dox-loaded PPro–TA capsules, Dox-loaded PArg–TA capsules, or free Dox at different drug dosages for 48 h at 37 °C. Data are shown as the mean ± standard deviation of six independent experiments.

the type of molecular interactions between PPeps and TA, and the thermodynamics thereof, showed that PPeps with different side chains interact with polyphenols via different supramolecular interactions. The strong interactions displayed between PArg or PPro and TA were then leveraged to assemble PPep–TA capsules that exhibited diverse physicochemical properties, structures, thicknesses, and stimuli-responsiveness due to the different interactions operating within the assemblies. For example, the PPep–TA capsules formed from PPeps with positive side chains exhibited pH-responsive charge reversal behavior, and the film thickness of the PArg–TA capsules was more than 10 times the thickness of the PPro–TA capsules. Importantly, PArg–TA coatings on particles could facilitate their cellular association and subsequent endosomal escape. These are beneficial properties for intracellular drug delivery. Furthermore, the Dox-loaded PPep–TA capsules displayed effective cell toxicity toward cancer cells. Whereas PArg was responsible for cell association and endosomal escape, the ability to form stable capsules and the loading of a drug, such as Dox, could be attributed to the adherence of TA to molecules. Hence, the reciprocal interactions between these different types of molecules, as well as their individual properties, could enable the design of functional materials for advanced applications. These PPN materials have good tunability and versatility, and customized structures for a range of functionalities could be engineered into the PPep-based assemblies by balancing various interactions.

ASSOCIATED CONTENT

Supporting Information

The Supporting Information is available free of charge at http://pubs.acs.org

Materials; characterization; cell culture; QCM analysis; ITC analysis; MOE docking; synthesis of calcium carbonate particles; formation of PPep–polyphenol capsules or particles; capsule disassembly experiments; permeability tests; cell association studies of PPep–TA particles via flow cytometry; cell association studies of PPep–TA particles via confocal microscopy; endosomal escape of PPep−TA particles; cytotoxicity assay of Dox-loaded PPep–TA capsules; MIRIBEL; ITC, NMR, UV–vis spectroscopy, FTIR spectroscopy, ζ-potential, drug release, and XTT data; 2D Ligand interaction diagrams; confocal and SEM images; chemical properties of PPeps (PDF)

AUTHOR INFORMATION

Corresponding Author

*fcaruso@unimelb.edu.au

Notes

The authors declare no competing financial interest.

ACKNOWLEDGMENT

This research was funded by the Australian Research Council (ARC) through the Discovery Project (DP200100713) scheme. F.C. acknowledges the award of a National Health and Medical Research Council Senior Principal Research Fellowship (GNT1135806). R.P.M.L. acknowledges the Netherlands Organisation for Scientific Research for a Rubicon postdoctoral fellowship (project 019.182EN.034). This work was performed in part at the Materials Characterisation and Fabrication Platform and the Bio21 Melbourne Protein Characterisation Platform at The University of Melbourne and the Victorian Node of the Australian National Fabrication Facility. We thank Dr Chan-Jin Kim and Dr Sukhvir Kaur Bhangu for helpful discussions, Yi Li for assistance with MOE simulation, and Dr Jiaying Song and Dr Yijiao Qu for assistance with experiments.

REFERENCES

(1) Lutz, J.-F.; Lehn, J.-M.; Meijer, E.; Matyjaszewski, K. From Precision Polymers to Complex Materials and Systems. *Nat. Rev. Mater.* **2016**, *1*, 16024.
(2) Zagorodko, O.; Arroyo-Crespo, J. J.; Nebot, V. J.; Vicent, M. J. Polypeptide-Based Conjugates as Therapeutics: Opportunities and Challenges. *Macromol. Biosci.* **2017**, *17*, 1600316.
(3) Deng, C.; Zhang, Q.; Guo, J.; Zhao, X.; Zhong, Z. Robust and Smart Polypeptide-Based Nanomedicines for Targeted Tumor Therapy. *Adv. Drug Delivery Rev.* **2020**, *160*, 199–211.
(4) Melnyk, T.; Dordevic, S.; Conejos-Sanchez, I.; Vicent, M. J. Therapeutic Potential of Polypeptide-Based Conjugates: Rational Design and Analytical Tools That Can Boost Clinical Translation. *Adv. Drug Delivery Rev.* **2020**, *160*, 136–169.
(5) Eimura, H.; Niwa, A.; Uchida, J.; Kato, T. Self-Assembly of Peptide-Containing Mesogens: Thermotropic Liquid-Crystalline Properties and Macroscopic Alignment of Amphiphilic Bioconjugates. *Bull. Chem. Soc. Jpn.* **2021,** *94*, 1588–1593.
(6) Delfi, M.; Sartorius, R.; Ashrafizadeh, M.; Sharifi, E.; Zhang, Y.; De Berardinis, P.; Zarrabi, A.; Varma, R. S.; Tay, F. R.; Smith, B. R. Self-Assembled Peptide and Protein Nanostructures for Anti-Cancer Therapy: Targeted Delivery, Stimuli-Responsive Devices and Immunotherapy. *Nano Today* **2021,** *38*, 101119.
(7) Skwarczynski, M.; Zhao, G.; Boer, J. C.; Ozberk, V.; Azuar, A.; Cruz, J. G.; Giddam, A. K.; Khalil, Z. G.; Pandey, M.; Shibu, M. A. Poly (amino Acids) as a Potent Self-Adjuvanting Delivery System for Peptide-Based Nanovaccines. *Sci. Adv.* **2020**, *6*, eaax2285.
(8) Sun, J.; Xiao, L.; Li, B.; Zhao, K.; Wang, Z.; Zhou, Y.; Ma, C.; Li, J.; Zhang, H.; Herrmann, A. Genetically Engineered Polypeptide Adhesive Coacervates for Surgical Applications. *Angew. Chem. Int. Ed.* **2021**, *60*, 23687–23694.
(9) Banskota, S.; Saha, S.; Bhattacharya, J.; Kirmani, N.; Yousefpour, P.; Dzuricky, M.; Zakharov, N.; Li, X.; Spasojevic, I.; Young, K. Genetically Encoded Stealth Nanoparticles of a Zwitterionic Polypeptide-Paclitaxel Conjugate Have a Wider Therapeutic Window than Abraxane in Multiple Tumor Models. *Nano Lett.* **2020**, *20*, 2396–2409.
(10) Pullen, S.; Tessarolo, J.; Clever, G. H. Increasing Structural and Functional Complexity in Self-Assembled Coordination Cages. *Chem. Sci.* **2021,** *12*, 7269–7293.
(11) Vazdar, M.; Heyda, J.; Mason, P. E.; Tesei, G.; Allolio, C.; Lund, M.; Jungwirth, P. Arginine "Magic": Guanidinium Like-Charge Ion Pairing from Aqueous Salts to Cell Penetrating Peptides. *Acc. Chem. Res.* **2018**, *51*, 1455–1464.
(12) Kwon, E. J.; Dudani, J. S.; Bhatia, S. N. Ultrasensitive Tumour-Penetrating Nanosensors of Protease Activity. *Nat. Biomed. Eng.* **2017**, *1*, 0054.
(13) Nelson, D. W.; Gilbert, R. J. Extracellular Matrix-Mimetic Hydrogels for Treating Neural Tissue Injury: A Focus on Fibrin, Hyaluronic Acid, and Elastin-Like Polypeptide Hydrogels. *Adv. Healthcare Mater.* **2021**, *10*, 2101329.
(14) Zhang, Y.; He, P.; Zhang, P.; Yi, X.; Xiao, C.; Chen, X. Polypeptides-Drug Conjugates for Anticancer Therapy. *Adv. Healthcare Mater.* **2021**, *10*, e2001974.
(15) Watson, E. E.; Angerani, S.; Sabale, P. M.; Winssinger, N. Biosupramolecular Systems: Integrating Cues into Responses. *J. Am. Chem. Soc.* **2021**, *143*, 4467–4482.
(16) Webber, M. J.; Appel, E. A.; Meijer, E.; Langer, R. Supramolecular Biomaterials. *Nat. Mater.* **2016**, *15*, 13–26.
(17) Aida, T.; Meijer, E.; Stupp, S. Functional Supramolecular Polymers. *Science* **2012**, *335*, 813–817.
(18) Mattia, E.; Otto, S. Supramolecular Systems Chemistry. *Nat. Nanotechnol.* **2015**, *10*, 111–119.
(19) Goor, O. J.; Hendrikse, S. I.; Dankers, P. Y.; Meijer, E. From Supramolecular Polymers to Multi-Component Biomaterials. *Chem. Soc. Rev.* **2017**, *46*, 6621–6637.
(20) Song, Z.; Han, Z.; Lv, S.; Chen, C.; Chen, L.; Yin, L.; Cheng, J. Synthetic Polypeptides: From Polymer Design to Supramolecular Assembly and Biomedical Application. *Chem. Soc. Rev.* **2017**, *46*, 6570–6599.
(21) Jeong, W.-j.; Kwon, S. h.; Lim, Y.-b. Modular Self-Assembling Peptide Platform with a Tunable Thermoresponsiveness via a Single Amino Acid Substitution. *Adv. Funct. Mater.* **2018**, *28*, 1803114.
(22) Garrett, M. C.; O'Shea, T. M.; Wollenberg, A. L.; Bernstein, A. M.; Hung, D.; Staarman, B.; Soto, H.; Deming, T. J.; Sofroniew, M. V.; Kornblum, H. I., Injectable Diblock Copolypeptide Hydrogel Provides Platform to Deliver Effective Concentrations of Paclitaxel to an Intracranial Xenograft Model of Glioblastoma. *PLoS One* **2020**, *15*, e0219632.
(23) Bravo-Anaya, L. M.; Garbay, B.; Nando-Rodríguez, J. L.; Ramos, F. C.; Ibarboure, E.; Bathany, K.; Xia, Y.; Rosselgong, J.; Joucla, G.; Garanger, E. Nucleic Acids Complexation with Cationic Elastin-Like Polypeptides: Stoichiometry and Stability of Nano-Assemblies. *J. Colloid Interface Sci.* **2019**, *557*, 777–792.
(24) Guan, X.; Guo, Z.; Lin, L.; Chen, J.; Tian, H.; Chen, X. Ultrasensitive pH Triggered Charge/Size Dual-Rebound Gene Delivery System. *Nano Lett.* **2016,** *16*, 6823–6831.
(25) Mogaki, R.; Hashim, P. K.; Okuro, K.; Aida, T. Guanidinium-Based "Molecular Glues" for Modulation of Biomolecular Functions. *Chem. Soc. Rev.* **2017**, *46*, 6480–6491.
(26) Guo, J.; Suma, T.; Richardson, J. J.; Ejima, H. Modular Assembly of Biomaterials Using Polyphenols as Building Blocks. *ACS Biomater. Sci. Eng.* **2019**, *5*, 5578–5596.
(27) Wu, D.; Zhou, J.; Creyer, M. N.; Yim, W.; Chen, Z.; Messersmith, P. B.; Jokerst, J. V., Phenolic-Enabled Nanotechnology: Versatile Particle Engineering for Biomedicine. *Chem. Soc. Rev.* **2021**, *50*, 4432–4483.
(28) Zhou, J.; Lin, Z.; Ju, Y.; Rahim, M. A.; Richardson, J. J.; Caruso, F. Polyphenol-Mediated Assembly for Particle Engineering. *Acc. Chem. Res.* **2020**, *53*, 1269–1278.

(29) Han, Y.; Lin, Z.; Zhou, J.; Yun, G.; Guo, R.; Richardson, J. J.; Caruso, F. Polyphenol-Mediated Assembly of Proteins for Engineering Functional Materials. *Angew. Chem. Int. Ed.* **2020**, *59*, 15618–15625.
(30) Shin, M.; Lee, H.-A.; Lee, M.; Shin, Y.; Song, J.-J.; Kang, S.-W.; Nam, D.-H.; Jeon, E. J.; Cho, M.; Do, M.; Park, S.; Lee, M. S.; Jang, J.-H.; Cho, S.-W.; Kim, K.-S.; Lee, H. Targeting Protein and Peptide Therapeutics to the Heart Via Tannic Acid Modification. *Nat. Biomed. Eng.* **2018**, *2*, 304–317.
(31) Tamerler, C.; Oren, E. E.; Duman, M.; Venkatasubramanian, E.; Sarikaya, M. Adsorption Kinetics of an Engineered Gold Binding Peptide by Surface Plasmon Resonance Spectroscopy and a Quartz Crystal Microbalance. *Langmuir* **2006**, *22*, 7712–7718.
(32) Zondlo, N. J. Aromatic–Proline Interactions: Electronically Tunable CH/π Interactions. *Acc. Chem. Res.* **2013**, *46*, 1039–1049.
(33) Kankare, J. Sauerbrey Equation of Quartz Crystal Microbalance in Liquid Medium. *Langmuir* **2002**, *18*, 7092–7094.
(34) Ross, P. D.; Subramanian, S. Thermodynamics of Protein Association Reactions: Forces Contributing to Stability. *Biochemistry* **1981**, *20*, 3096–3102.
(35) Archer, W. R.; Schulz, M. D. Isothermal Titration Calorimetry: Practical Approaches and Current Applications in Soft Matter. *Soft Matter* **2020**, *16*, 8760–8774.
(36) Araki, M.; Matsumoto, S.; Bekker, G.-J.; Isaka, Y.; Sagae, Y.; Kamiya, N.; Okuno, Y. Exploring Ligand Binding Pathways on Proteins Using Hypersound-Accelerated Molecular Dynamics. *Nat. Commun.* **2021**, *12*, 2793.
(37) Attique, S. A.; Hassan, M.; Usman, M.; Atif, R. M.; Mahboob, S.; Al-Ghanim, K. A.; Bilal, M.; Nawaz, M. Z. A Molecular Docking Approach to Evaluate the Pharmacological Properties of Natural and Synthetic Treatment Candidates for Use against Hypertension. *Int. J. Environ. Res. Public Health* **2019**, *16*, 923.
(38) Richardson, J. J.; Maina, J. W.; Ejima, H.; Hu, M.; Guo, J.; Choy, M. Y.; Gunawan, S. T.; Lybaert, L.; Hagemeyer, C. E.; De Geest, B. G. Versatile Loading of Diverse Cargo into Functional Polymer Capsules. *Adv. Sci.* **2015**, *2*, 1400007.
(39) Björnmalm, M.; Cui, J.; Bertleff-Zieschang, N.; Song, D.; Faria, M.; Rahim, M. A.; Caruso, F. Nanoengineering Particles through Template Assembly. *Chem. Mater.* **2017**, *29*, 289–306.
(40) Ejima, H.; Richardson, J. J.; Liang, K.; Best, J. P.; van Koeverden, M. P.; Such, G. K.; Cui, J.; Caruso, F. One-Step Assembly of Coordination Complexes for Versatile Film and Particle Engineering. *Science* **2013**, *341*, 154–157.
(41) Rahim, M. A.; Kempe, K.; Müllner, M.; Ejima, H.; Ju, Y.; van Koeverden, M. P.; Suma, T.; Braunger, J. A.; Leeming, M. G.; Abrahams, B. F.; Caruso, F. Surface-Confined Amorphous Films from Metal-Coordinated Simple Phenolic Ligands. *Chem. Mater.* **2015**, *27*, 5825–5832.
(42) Deng, C.; Wu, J.; Cheng, R.; Meng, F.; Klok, H.-A.; Zhong, Z. Functional Polypeptide and Hybrid Materials: Precision Synthesis Via α-Amino Acid N-Carboxyanhydride Polymerization and Emerging Biomedical Applications. *Prog. Polym. Sci.* **2014**, *39*, 330–364.
(43) Faria, M.; Björnmalm, M.; Thurecht, K. J.; Kent, S. J.; Parton, R. G.; Kavallaris, M.; Johnston, A. P.; Gooding, J. J.; Corrie, S. R.; Boyd, B. J.; Thordarson, P.; Whittaker, A. K.; Stevens, M. M.; Prestidge, C. A.; Porter, C. J. H.; Parak, W. J.; Davis, T. P.; Crampin, E. J.; Caruso, F. Minimum Information Reporting in Bio–Nano Experimental Literature. *Nat. Nanotechnol.* **2018**, *13*, 777–785.

Insert Table of Contents artwork here